Supporting Information

for

Characterization of Parallel β-sheets at Interfaces by Chiral Sum Frequency Generation Spectroscopy

Li Fu,[#] *Zhuguang Wang, Brian T. Psciuk, Dequan Xiao*[†]*, Victor S. Batista, and Elsa C.Y. Yan**

Department of Chemistry, Yale University, 225 Prospect Street, New Haven, CT 06520

†Current Address: Department of Chemistry and Chemical Engineering, University of New Haven, West Haven, CT 06516

#Current Address: Pacific Northwest National Laboratory, 902 Battelle Boulevard, Richland, WA 99352

1. Materials and methods

hIAPP was synthesized and purified by the W.M. Keck Biotechnology Resource Laboratory of Yale University (New Haven, CT). The synthetic parallel *β*-sheet peptide SJM2116a was prepared as described in previous literatures.[1] The lyophilized hIAPP and SJM2116a peptides were dissolved in deionized water at the concentration ~2 μg/ml, and were aliquoted into vials, which were frozen as stock solutions in liquid nitrogen and stored at -80°C. We took the SFG spectra of hIAPP using two configurations: (1) at the air/water interface and (2) on glass slide surface (18 × 18 mm, Fisher Scientific, microscope cover glass, mainly SiO_2),

which was cleaned by surface plasma. For the SFG experiments performed at the air/water interface, we added the hIAPP stock solution of 50 μL using a Hamilton micro-syringe to a Teflon beaker in a diameter of 4 cm that contained 4.5 ml phosphate buffer (10 mM, pH 7.4). The final bulk concentration of hIAPP was 4 μg/mL (~1 μM). The surface coverage of hIAPP is close to 100% at this bulk concentration.[2] DPPG (431 μM) was added as a solution in a mixture of chloroform and methanol (3:1) using a Hamilton micro-syringe at a final surface density of 110 $Å^2$ per lipid molecule to induce aggregation of hIAPP. Our previous work showed that hIAPP aggregates in 10 hours upon addition of DPPG under our experimental conditions. For the samples on glass slides, we spread ~10 μL of ~10 μM hIAPP stock solution and then 4 μL of ~0.4 μM DPPG onto the glass slide forming a spot with a diameter ~1 cm. Subsequently, we dried the glass slide overnight. We also took the SFG spectra of the SJM2116a peptide at the glass slide surfaces, which is prepared by drop the peptide solution onto glass slide and dried overnight.

We obtained the chiral SFG spectra with the *psp* polarization settings (*p*-polarized SFG, *s*-polarized visible, and *p*-polarized IR) using our broad bandwidth SFG spectrometer,[3] with an acquisition time of 10 min. The raw SFG spectra were processed, as described, including the steps of removing the contribution from cosmic rays, subtracting background, calibrating the wavenumber, and normalizing to the IR power.[3]

2. Experimental SFG spectrometer

We used a broad-bandwidth SFG spectrometer setup, which was described in detail in Ma *et al*. The spectrometer consists of a 6-W regenerative amplifier (5 kHz, Spitfire Pro, Spectra Physics, CA) seeded by a Ti:sapphire oscillator (Mai Tai XF, 120 fs, Spectra-Physics) and pumped by two diode Neodymium-doped yttrium lithium fluoride (Nd:YLF) lasers (Empower,

Spectra Physics). One half of the 6-W passed through a home-built pulse shaper to produce 800-nm pulses with a bandwidth of 7 cm^{-1}, and the other half pumped an optical parametric amplifier (OPA) (TOPAS-C, Spectra-Physics, CA) to generate broad-bandwidth IR pulses. The power of the 800-nm beam at the sample stage was ~80 mW, and the power of the IR beam at the sample stage was ~10 mW. The incident angles for the 800-nm and IR beams were 56° and 69°, respectively. The SFG signal generated from the sample was filtered and then dispersed by a monochromator (Acton, SP-2558, Princeton Instruments) before being detected by a CCD (Spec-10:400BR, Princeton Instruments).

3. Supplementary Data

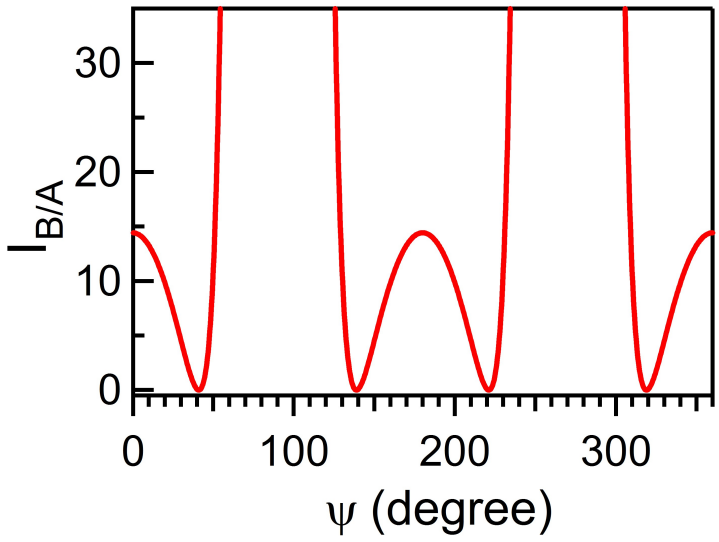

Figure S1. Intensity ratio of amide I B to amide I A mode in the *psp* spectrum as a function of twist angle (ψ). Data replotted from Ref. [4].

Table S1. Spectral parameters obtained by fitting the amide I bands in Figure 3.

	χ_{NR} (a.u.)	-0.0013 ± 0.005
A mode	ω_A (cm^{-1})	1661.9 ± 0.9
	A_A (a.u.)	0.5 ± 0.2
	Γ_A (a.u.)	8.0 ± 2.4
B mode	ω_B (cm^{-1})	1635.8 ± 0.3
	A_B (a.u.)	11.6 ± 0.3
	Γ_B (a.u.)	18.0 ± 0.4

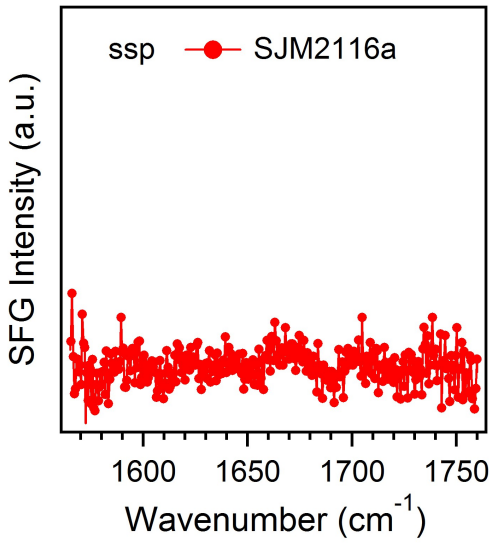

Figure S2. The *ssp* SFG spectrum of the parallel β-sheet peptide 1 in the amide I region at the glass slide surface.

4. Derivation of the effective susceptibility as a function of hyperpolarizability elements

4.1 Chiral SFG

Under the *psp* polarization setting, the effective susceptibility can be expressed as:[5]

$$\begin{aligned}\chi_{psp}^{(2)} &= L_{zz}(\omega_{SFG})L_{yy}(\omega_{VIS})L_{xx}(\omega_{IR})\sin\alpha_{SFG}\cos\alpha_{IR}\chi_{zyx}^{(2)} \\ &- L_{xx}(\omega_{SFG})L_{yy}(\omega_{VIS})L_{zz}(\omega_{IR})\cos\alpha_{SFG}\sin\alpha_{IR}\chi_{xyz}^{(2)}\end{aligned} \quad \text{(S1)}.$$

Equation (S2) can be simplified further if the Raman polarizability is symmetric, which is often the case when there is no electronic resonance. Under such a condition, $\chi_{xyz} = \chi_{yxz}$. Since the C_∞ point group encompasses the C_4 subgroup, imposition of $x \rightarrow -y$ and $y \rightarrow x$ yields $\chi_{xyz} = \chi_{-yxz} = -\chi_{yxz} = -\chi_{xyz}$, and thus, $\chi_{xyz} = 0$. Therefore, under vibrationally resonant and electronically non-resonant conditions, Equation (S1) can be approximated as

$$\chi_{psp}^{(2)} = L_{zz}(\omega_{SFG})L_{yy}(\omega_{VIS})L_{xx}(\omega_{IR})\sin\alpha_{SFG}\cos\alpha_{IR}\chi_{zyx}^{(2)} = L_{zyx}\chi_{zyx}^{(2)} \quad \text{(S2)}.$$

The $\chi_{IJK}^{(2)}$ tensor elements can be expressed in terms of the β_{ijk} tensor elements using the Euler transformation:

$$\chi_{IJK,q}^{(2)} = N_S \sum_{i,j,k} \left\langle R_{Ii} R_{Jj} R_{Kk} \right\rangle \beta_{ijk,q} \quad \text{(S3)},$$

where I, J, K are the laboratory coordinates (x, y, z) and i, j, k are molecular coordinates (a, b, c); N_S is the number density of the molecular moiety under study; and R_{Ii}, R_{Jj}, and R_{Kk} are elements of the z-y-z rotational transformation matrix connecting the molecular coordinates to the laboratory coordinates.

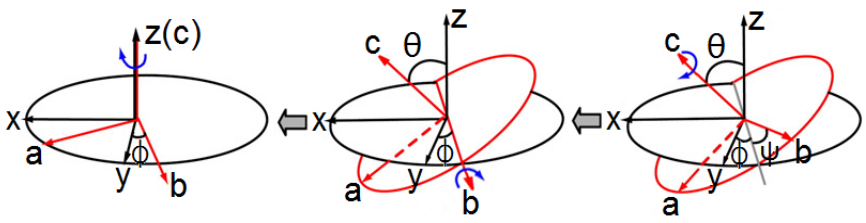

$$\begin{pmatrix} \cos\phi & -\sin\phi & 0 \\ \sin\phi & \cos\phi & 0 \\ 0 & 0 & 1 \end{pmatrix} \bullet \begin{pmatrix} \cos\theta & 0 & \sin\theta \\ 0 & 1 & 0 \\ -\sin\theta & 0 & \cos\theta \end{pmatrix} \bullet \begin{pmatrix} \cos\psi & -\sin\psi & 0 \\ \sin\psi & \cos\psi & 0 \\ 0 & 0 & 1 \end{pmatrix} =$$

$$\begin{pmatrix} \cos\phi\cos\theta\cos\psi - \sin\phi\sin\psi & -\sin\phi\cos\psi - \cos\phi\cos\theta\sin\psi & \cos\phi\sin\theta \\ \sin\phi\cos\theta\cos\psi + \cos\phi\sin\psi & \cos\phi\cos\psi - \sin\phi\cos\theta\sin\psi & \sin\phi\sin\theta \\ -\sin\theta\cos\psi & \sin\theta\sin\psi & \cos\theta \end{pmatrix}$$

Scheme S1. *z-y-z* Euler transformation from the molecular coordinates (*a*, *b*, *c*) to laboratory coordinates (*x*, *y*, *z*). The Euler transformation matrices on the right-hand side are yielded by the multiplication of the three rotational matrices on the left-hand side corresponding to the rotational operations.

Using the *z-y-z* transformation (Scheme S1), $\chi^{(2)}_{zyx}$ can be expressed as a function of (θ, ψ, ϕ). After averaging the in-plane rotation angle (ϕ) by the integration over 0 to 2π for an isotropic interface on the *x-y* plane,

$$\chi^{(2)}_{psp} = L_{zyx}\chi^{(2)}_{zyx} = -\frac{L_{zyx}}{2} N_S \times \begin{Bmatrix} \langle \cos^2\theta \rangle (\beta_{cab} - \beta_{cba}) \\ + \langle \sin^2\theta \sin^2\psi \rangle (\beta_{bca} - \beta_{bac}) \\ + \langle \sin^2\theta \cos^2\psi \rangle (\beta_{abc} - \beta_{acb}) \\ + \langle \sin^2\theta \sin\psi \cos\psi \rangle (\beta_{aac} - \beta_{aca} - \beta_{bbc} + \beta_{bcb}) \\ + \langle \sin\theta \cos\theta \sin\psi \rangle (\beta_{bab} - \beta_{bba} - \beta_{cac} + \beta_{cca}) \\ + \langle \sin\theta \cos\theta \cos\psi \rangle (-\beta_{aab} + \beta_{aba} - \beta_{cbc} + \beta_{ccb}) \end{Bmatrix} \quad \text{(S4)}.$$

In the case of C_2 symmetry, $\beta_{abc} = \beta_{bac}$, $\beta_{cba} = \beta_{bca}$, $\beta_{acb} = \beta_{cab}$, $\beta_{cbc} = \beta_{bcc}$, $\beta_{aba} = \beta_{baa}$, β_{bbb}, β_{aab}, β_{ccb}. Equation (S4) can be further simplified as:

$$\chi_{psp}^{(2)} = -\frac{L_{zyx}}{2} N_S \begin{Bmatrix} \langle \cos^2\theta \rangle (\beta_{cab} - \beta_{cba}) + \langle \sin^2\theta \sin^2\psi \rangle (\beta_{bca} - \beta_{bac}) \\ + \langle \sin^2\theta \cos^2\psi \rangle (-\beta_{acb} + \beta_{abc}) \\ + \langle \sin\theta \cos\theta \cos\psi \rangle (-\beta_{aab} + \beta_{aba} - \beta_{cbc} + \beta_{ccb}) \end{Bmatrix} \quad \text{(S5).}$$

Previously, we discussed the surface-specificity of chiral SFG signals.[6] We have shown that with the electric-dipole approximation and in the absence of electronic resonance, chiral SFG is surface specific, as long as the interface has C_∞ symmetry and the bulk is isotropic lacking a reflection plane perpendicular to the interface. All these requirements are met under our experimental conditions. Therefore, the observed chiral SFG signal is generated from the interface in our study.

4.2 Achiral SFG

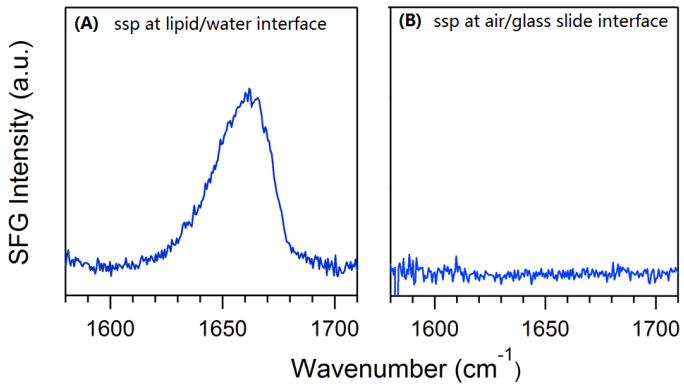

Figure S3. The achiral ssp SFG spectra in the amide I region of (A) The hIAPP aggregates at the lipid/water interface, and (B) The hIAPP aggregates on the glass slide interface.

The conventional (achiral) SFG spectra taken using the *ssp* polarization (*s*-polarized SFG, *s*-polarized visible, and *p*-polarized IR) in the amide I region of hIAPP aggregates show signal at

1660 cm^{-1} at the air/water interface and is silent on the glass slide (Figure S3), which is due to effects of orientation shown as below.

Similar as the chiral SFG, using the *z-y-z* transformation (Scheme S1), the achiral $\chi_{ssp}^{(2)}$ can also be expressed as a function of (θ, ψ, ϕ). After averaging the in-plane rotation angle (ϕ) by the integration over 0 to 2π for an isotropic interface on the *x-y* plane,

$$\chi_{ssp}^{(2)} = L_{yyz}\chi_{yyz}^{(2)} = \frac{L_{yyz}}{2}N_S$$
$$\left\{\begin{array}{l}
\langle\sin^2\theta\cos\theta\rangle(\beta_{ccc}) + \langle\cos\theta\rangle(\beta_{aac}+\beta_{bbc}) \\
-\langle\sin^2\theta\cos\theta\sin^2\psi\rangle(\beta_{bbc}+\beta_{bcb}+\beta_{cbb}) \\
-\langle\sin^2\theta\cos\theta\cos^2\psi\rangle(\beta_{aac}+\beta_{aca}+\beta_{caa}) \\
+\langle\sin^2\theta\cos\theta\sin\psi\cos\psi\rangle(\beta_{abc}+\beta_{acb}+\beta_{bac}+\beta_{bca}+\beta_{cab}+\beta_{cba}) \\
+\langle\sin\theta\sin\psi\rangle(\beta_{bbb}+\beta_{aab}-\beta_{bcc}-\beta_{cbc}) \\
+\langle\sin\theta\cos\psi\rangle(-\beta_{aaa}-\beta_{bba}+\beta_{acc}+\beta_{cac}) \\
+\langle\sin^3\theta\sin\psi\rangle(-\beta_{aab}-\beta_{aba}-\beta_{baa}+\beta_{bcc}+\beta_{cbc}+\beta_{ccb}) \\
+\langle\sin^3\theta\cos\psi\rangle(\beta_{abb}+\beta_{bab}+\beta_{bba}-\beta_{acc}-\beta_{cac}-\beta_{cca}) \\
+\langle\sin\theta^3\sin^3\psi\rangle(-\beta_{bbb}+\beta_{aab}+\beta_{aba}+\beta_{baa}) \\
+\langle\sin\theta^3\cos^3\psi\rangle(\beta_{aaa}-\beta_{abb}-\beta_{bab}-\beta_{bba})
\end{array}\right\} \quad \text{(S6)}$$

For the amide I bands, the *A* mode has

$$\chi_{ssp,A}^{(2)} = L_{yyz}\chi_{yyz,A}^{(2)} = \frac{L_{yyz}}{2}N_S\left\{\begin{array}{l}2\langle\sin^2\theta\cos\theta\sin\psi\cos\psi\rangle\beta_{acb} + \langle\sin\theta\sin\psi\rangle(\beta_{bbb}+\beta_{aab}) \\ +\langle\sin^3\theta\sin\psi\rangle(-\beta_{aab}+\beta_{ccb}) + \langle\sin\theta^3\sin^3\psi\rangle(-\beta_{bbb}+\beta_{aab})\end{array}\right\} \quad \text{(S7)},$$

and the *B* mode has

$$\chi_{ssp,B}^{(2)} = L_{yyz}\chi_{yyz,B}^{(2)} = L_{yyz}N_S\left\{\langle\sin^2\theta\cos\theta\sin\psi\cos\psi\rangle(\beta_{abc}+\beta_{bca}) - \langle\sin\theta\cos^2\theta\sin\psi\rangle\beta_{bcc}\right\} \quad \text{(S8)}.$$

At the lipid water interface, the θ = 90°. Therefore, the ssp SFG spectrum shows only *A* mode signals without *B* mode signals. At the glass slides, where θ = 90° and ψ = 0°, the ssp SFG spectrum exhibits neither *A* nor *B* mode signals.

5. Contribution of turn structures to the ~1660 cm^{-1} peak in hIAPP spectra

In conventional vibrational spectroscopy, turn structures often show characteristic peaks at ~1660 cm^{-1} in the amide I region. However, it is unlikely that this peak can be detected by chiral SFG, which is sensitive to macroscopic chirality. As experimental evidence, we refer to the work by Chen and coworkers, who were the first to observe the chiral SFG vibrational signals from macromolecular interfacial structures.[7] They took the *psp* (the same polarization that we used) spectrum of tachyplesin I, a model peptide with anti-parallel β-sheet and turn structures. While they observed two characteristic peaks for anti-parallel β-sheet in the *psp* spectra (1633 cm^{-1} and 1688 cm^{-1}), they did not observe the characteristic peak for turn structures (~1660 cm^{-1}). There are two possible reasons for the invisibility of turn structures in chiral SFG. First, only 3 to 4 residues are involved in the β-turn structure. The sequence is so short that it is questionable whether it can meet the requirement of "macroscopic chirality" for chiral SFG to detect.[8] Second, even if turn structures can give chiral SFG amide I signal, the contribution to the ~1660 cm^{-1} peak is expected to be negligible compared to the parallel β-sheet structure in hIAPP. Of the total 37 amino acids in hIAPP, only 4 are involved in the turn structure, but 20 in parallel β-sheet structure. SFG intensity is directly proportional to the square of the surface population. Thus, when only surface population is taken into account, the contribution to the SFG intensity from the turn structure is only ~ 4% ($4^2/20^2 = 0.04$) of that from parallel β-sheets. Therefore, the intensity from the turn structures is expected to be much weaker than that from parallel β-sheets in hIAPP.

6. Characterization of peptide 1

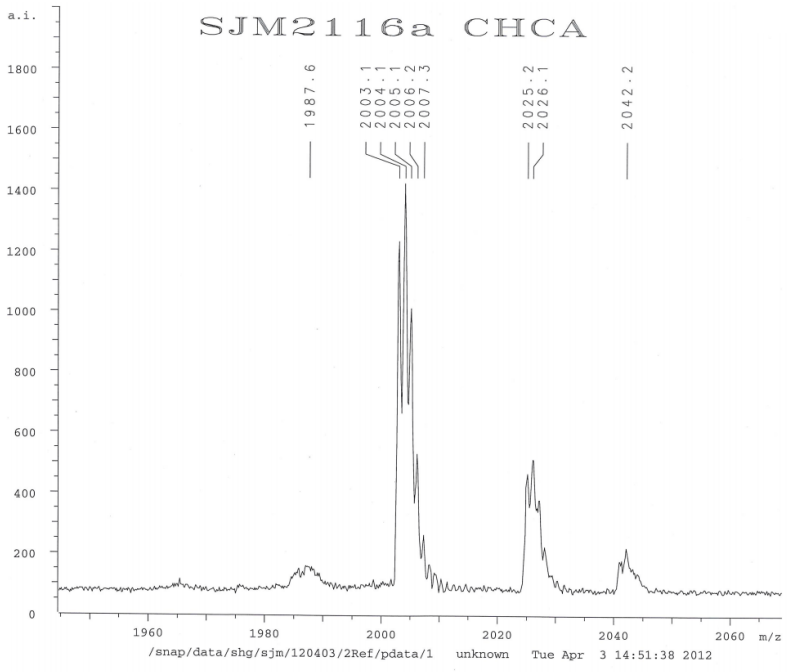

Figure S4. The MALDI of peptide 1.

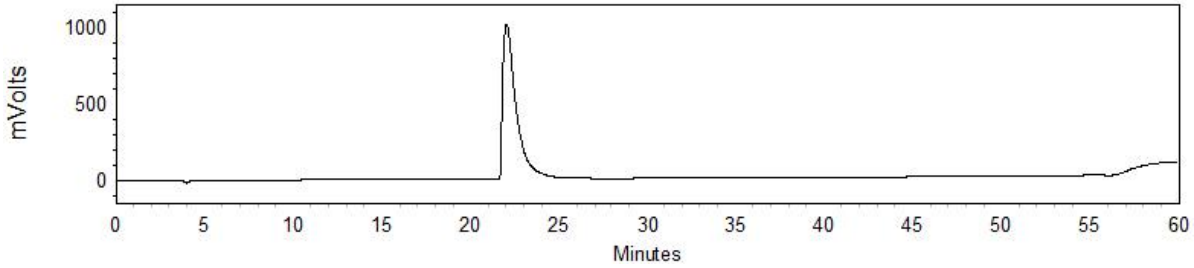

Figure S5. The purity check for peptide 1 using HPLC at 220 nm using C5 column.

References:

1. Freire, F.; Gellman, S. H. Macrocyclic Design Strategies for Small, Stable Parallel Beta-Sheet Scaffolds. *J Am Chem Soc* **2009**, *131*, 7970-+.
2. Lopes, D. H. J.; Meister, A.; Gohlke, A.; Hauser, A.; Blume, A.; Winter, R. Mechanism of Islet Amyloid Polypeptide Fibrillation at Lipid Interfaces Studied by Infrared Reflection Absorption Spectroscopy. *Biophys. J.* **2007**, *93*, 3132-3141.
3. Ma, G.; Liu, J.; Fu, L.; Yan, E. C. Y. Probing Water and Biomolecules at the Air-Water Interface with a Broad Bandwidth Vibrational Sum Frequency Generation Spectrometer from 3800 to 900 Cm(-1). *Appl Spectrosc* **2009**, *63*, 528-537.
4. Xiao, D. Q.; Fu, L.; Liu, J.; Batista, V. S.; Yan, E. C. Y. Amphiphilic Adsorption of Human Islet Amyloid Polypeptide Aggregates to Lipid/Aqueous Interfaces. *J. Mol. Biol.* **2012**, *421*, 537-547.
5. Wang, H. F.; Gan, W.; Lu, R.; Rao, Y.; Wu, B. H. Quantitative Spectral and Orientational Analysis in Surface Sum Frequency Generation Vibrational Spectroscopy (Sfg-Vs). *Int. Rev. Phys. Chem.* **2005**, *24*, 191-256.
6. Yan, E. C. Y.; Fu, L.; Wang, Z.; Liu, W. Biological Macromolecules at Interfaces Probed by Chiral Vibrational Sum Frequency Generation Spectroscopy. *Chem. Rev.* **2014**, *114*, 8471-8498.
7. Wang, J.; Chen, X. Y.; Clarke, M. L.; Chen, Z. Detection of Chiral Sum Frequency Generation Vibrational Spectra of Proteins and Peptides at Interfaces in Situ. *Proc. Natl. Acad. Sci. U. S. A.* **2005**, *102*, 4978-4983.
8. Haupert, L. M.; Simpson, G. J. Chirality in Nonlinear Optics. *Annu. Rev. Phys. Chem.* **2009**, *60*, 345-365.